FPCM-9 (2008)
The 9th International Conference on Flow Processes in Composite Materials
Montréal (Québec), Canada
8 ~ 10 July 2008

BUBBLE FORMATION AND MOTION IN NON-CRIMP FABRICS WITH PERTURBED BUNDLE GEOMETRY

T. Staffan Lundström[1], Vilnis Frishfelds[2, 3], Andris Jakovics[2]

[1] *Division of fluid dynamics, Luleå University of Technology, SE-971 87, Luleå, Sweden*
[2] *University of Latvia, Zellu 8, Riga LV-1002, Latvia*
[3] *Corresponding author's Email: frishfelds@latnet.lv*

SUMMARY: The behaviour of the fluid front during impregnation of non-crimp fabrics has been considered. Particular attention is paid to creation of bubbles at the fluid front and a virtual 3D model mimicking biaxial fabrics has been build for this purpose. The saturated fluid flow is governed by Navier-Stokes Equations and Darcy law while capillary pressure has been accounted for at the fluid flow front. Continuity is furthermore preserved. The influence of perturbation in the bundle geometry has been investigated where it turns out that local correlations of dimensions of neighbouring gaps formed between the bundles are of highest importance. Focus is set on inter-bundle bubbles, where a previously built model for bubble dynamics is used based on a probabilistic approach for bubbles moving, slitting, merging, dying, and shaping. The obtained void fractions of inter-bundle bubbles at different levels of vacuum applied at the liquid flow front is compared to those from real mouldings with rather good conformity.

KEYWORDS: non-crimp fabrics, impregnation, bubbles

INTRODUCTION

In non-crimp fabrics the fibers are collected in straight bundles being placed parallel in layers that are stitched together to form a strong reinforcement [1]. The geometrical result is a porous medium having dual scale porosity. The flow generated during impregnation therefore takes place on at least two scales, the fiber scale 0.01 mm and the fiber bundle scale 0.1 mm. At the wetting front the higher capillary forces together with the larger resistance to flow within the bundles thus compete with the lower resistance to flow and lower capillary forces in the inter bundle channels. This suggests that the leading front can be in the small intra bundle channels as well as in the large inter bundle channels [2] while in the part that is impregnated the velocity of the liquid resin in the inter bundle channels is orders of magnitude higher than the velocity within the bundles. There is also a natural variation in the distribution of the fibers within a bundle implying that the velocity can vary a lot within a fiber bundle, as well, at the wetting flow front and in the bulk. The fiber bundles in their turn are often assembled in an organized way by stitching

techniques but their exact positions will deviate from a perfect pattern due to statistical variations and manufacturing induced flaws. Hence also the averaged velocity in the inter bundles channels will vary as a function of spatial coordinate. All in all, we may anticipate an inhomogeneous flow front on several scales and thus a large risk for air to be entrapped. Once being formed the transport of the bubbles during processing has a large influence on the distribution of voids in the final composite. During processing, enclosed gas (or volatile components in the resin) may move as bubbles or dissolve into the resin as molecules. One evidence of such transports was reported in [3] were laminates with different lengths were manufactured at identical processing conditions and by letting the resin flow from one side of the mold to the other in an overall parallel flow. Studies of micrographs showed that the leading liquid flow front was followed by a fully saturated flow front where the latter had a somewhat lower speed. It is well known that the quality of composites made by RTM are highly improved when, during the impregnation, the inlet driving pressure is assisted by a reduced pressure (vacuum) on the outlet side of the mold [3, 4]. This positive result can be explained by assuming that bubbles are formed at the liquid flow front. Then, a lower pressure at the flow front makes less air available to be entrapped resulting in smaller bubbles in the liquid resin as compared to an impregnation without vacuum assistance. Other methods to improve the quality is to impregnate the fabric at an optimal capillary number [5], avoid dry spots [6], apply a pressure on the resin after filling [3, 7] and use matching material combinations [3].

We will here present a model for the formation and transport of bubbles during impregnation of non-crimp fabrics. The work is based on a series of papers published regarding transport of bubbles and the flow through the part of the fabric already impregnated. Numerical description of motion of fluid front and creation of bubbles behind the front is a challenging task in impregnation of composite materials because of the rather complicated arrangement of the fibers as described above. At a glance the fiber structure looks organized but there are high local perturbations which change notably the permeability of fabrics [8]. Moreover, previous studies have shown that spatial correlations of local perturbations of bundle arrangement are of significant importance for the detailed flow. Perturbations exist both in fiber arrangement in the bundles and also in bundle arrangement in the fabrics. In the current paper this latter influence will be discussed in the context of bubble creation at the fluid front.

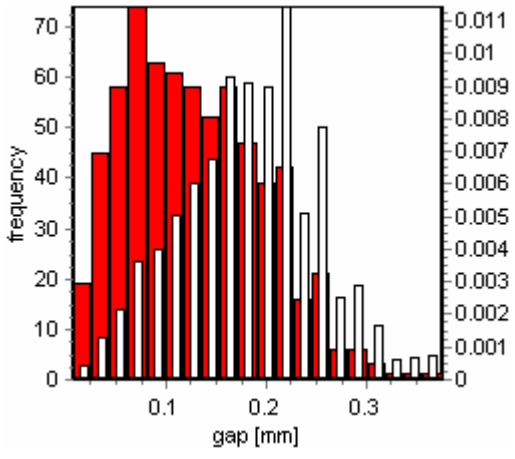

Fig. 1 Distribution of gap size (colour) and associated permeability (white).

NUMERICAL MODEL

A 3D numerical model is built for the impregnation of non-crimp fabrics. The model is based on a network model previously developed for fully impregnated fabrics [8] but by now also considering the flow through the bundles. The system is divided into an arbitrary number of layers each having an arbitrary primary orientation. It could, for instance be layers of biaxial or triaxial fabrics. Periodic boundary conditions are assumed in the direction normal to the layers, i.e., uppermost and lowermost layer are assumed to be laid side by side. The perturbed local positions of the fibre bundles are obtained by a Monte Carlo method [8] taking into account typical correlation parameters of the real fabrics obtained by an automatic recognition technique [9]. One result of this is that the gap size changes considerably throughout the fabrics, as exemplified in Fig. 1. One example of a top view that has been used to obtain the numerical shape of biaxial fabrics is illustrated in Fig. 2 where the two uppermost layers are shown. For the numerical modelling the bundles and gaps are furthermore divided into smaller elements with a length equal to average spacing of the bundles in the layer. It is moreover assumed that the cross-section of the channels has a parabolic shape as shown in the right-bottom corner of Fig. 2. In addition, biaxial fabrics have threads going through appropriate gaps and possible crossing fibres moving from one bundle to another as indicated in Fig. 2. It is assumed that all bundles have an equal shape and any perturbations in the fibre structure within the bundle are neglected.

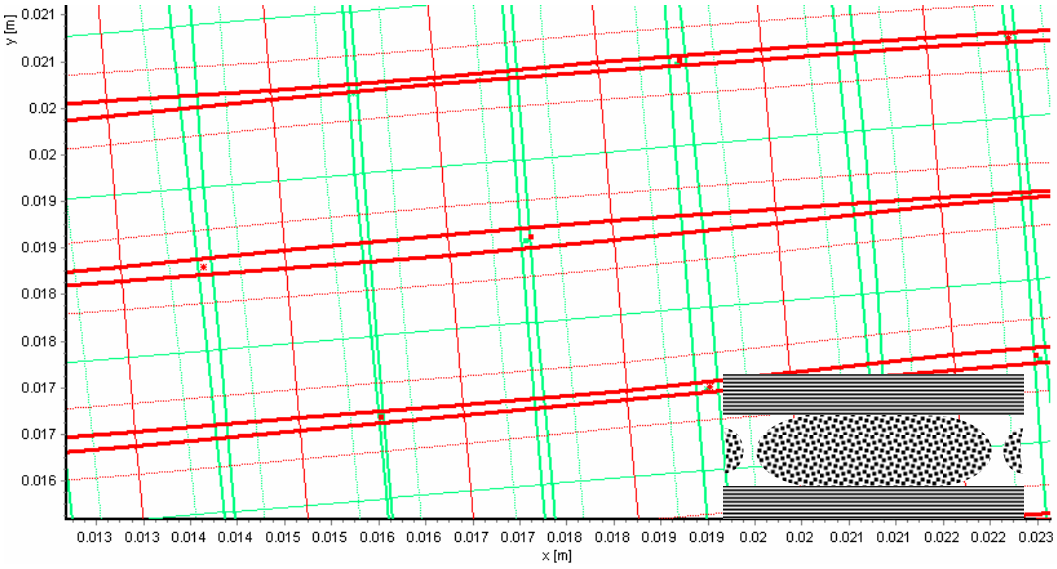

Fig. 2 Fragment of the top view of finite volumes of bundles and gaps in the perturbed biaxial fabrics with two uppermost layers. Threads and possible crossings are showed by small rectangles and stars, respectively. Typical cross-section of the bundle is shown at right-bottom corner.

As the speed of impregnation is extremely low Darcy flow is assumed in the load. Dynamic viscosity η is approximated as linearly dependent on volume fraction c of liquid at that position:

$$\mathbf{v} = \frac{K}{\eta(c)}\nabla P, \qquad \eta(c) = c\eta_{liq} + (1-c)\eta_{gas}, \tag{1}$$

where **v** is flow of the mixture, K –permeability, P – pressure, η_{liq}, η_{gas} are the dynamic viscosity in the pure liquid and gas and notice that the orientation of the fabric with respect to the pressure gradient can be arbitrary. Because the dynamic viscosity in gases generally is much smaller than in liquids, the resulting pressure variation in the gaseous phase is negligible. The values of the permeability in the elementary gaps are taken from 3D CFD calculations performed in [10] of the full Navier-Stokes Equations. These values depend on gap size, gap shape, layer spacing, presence or absence of thread or crossing at that place. The permeability inside the bundle depends primarily whether the flow is longitudinal ($\parallel$), i.e., in parallel to fibres or perpendicular to them ($\perp$). Usually it is much higher in the longitudinal case. These permeabilities are taken from unperturbed solutions from hexagonal packing [11]:

$$K_{\parallel} = \frac{8}{71}\left(\frac{r_p}{\Pi}\right)^2 (1-\Pi)^3, \qquad K_{\perp} = \frac{16}{9\pi}\sqrt{\frac{3}{2}} r_p^2 \left(\sqrt{\frac{\Pi_{\max}}{\Pi}} - 1\right)^{\frac{3}{2}}, \tag{2}$$

where Π is the fibre volume fraction in the bundle, $\Pi_{\max} = \pi/\left(2\sqrt{3}\right)$ – maximal volume fraction in the bundle, r_p – radius of the fibres. By no doubt perturbation in the fibre geometry largely influence both the permeability and the creation of bubbles especially within the bundles but this effect is neglected in this paper. The approximation of an additional pressure, the capillary pressure at liquid-gas interface is approximated by:

$$P_c = -\frac{\pi\sigma_{LG}}{2r_p}(1+\cos\theta), \tag{3}$$

where σ_{LG} is surface tension of the liquid-gas interface, θ - contact angle at the fibres. This quantity acts as a wetting force which helping the impregnation of the interior of the bundles. However, if the size of the fibres is as small as about 7 μm in radius then the wetting phase extends over several cells and the here used algorithms do not work well and additional considerations should be included [12]. A more detailed description of the liquid-gas interface inside the fibre bundles and around bubbles is presented in [13] by a lattice-gas analysis. The solution of the pressure in Eq. (1) is obtained by a 3D finite volume method. The elements have utmost 4 neighbours within the layer and an arbitrary number in the layers above and below. The transport to the neighbouring layers is calculated based both on the area of the contact face and the position. The concentration at faces of finite volumes is taken into account, too, in addition to the average concentration of the finite volume.

The liquid transport is derived from the fluxes (1) and the concentration at the element interfaces:

$$\frac{\partial c}{\partial t} + (\mathbf{v}\nabla)\, c = 0, \tag{4}$$

where diffusive transport is currently neglected. Air inclusions formed at the fluid front are treated as bubbles. There could be both inter-bundle and intra-bundle bubbles. The transport of the first type is determined by the Monte-Carlo method developed in [14]. Here, the bubbles jump from one inter-bundle site to a neighbouring one is based on transition probability. The transition probability is assumed to depend on bubble radius, fluxes in respective directions and cross-sectional size and shape also in respective directions. The bubble volume V_b is calculated by Clausius-Clapeyron law with known molar amount ν of gas inclusion:

$$\frac{PV_b}{\nu} = const\,. \tag{5}$$

Thus, the size of the bubble decreases as the front moves ahead because of increasing pressure that helps to move the bubble. Additionally, splitting of large bubbles and joining of bubbles is accounted for. Usually, the smaller bubbles move approximately as fast as the fluid front. Hence, there is high probability that they will reach fluid front not long after their appearance. The situation is different for bubbles that can be trapped in some of the constrictions in the reinforcement and reside there for a while.

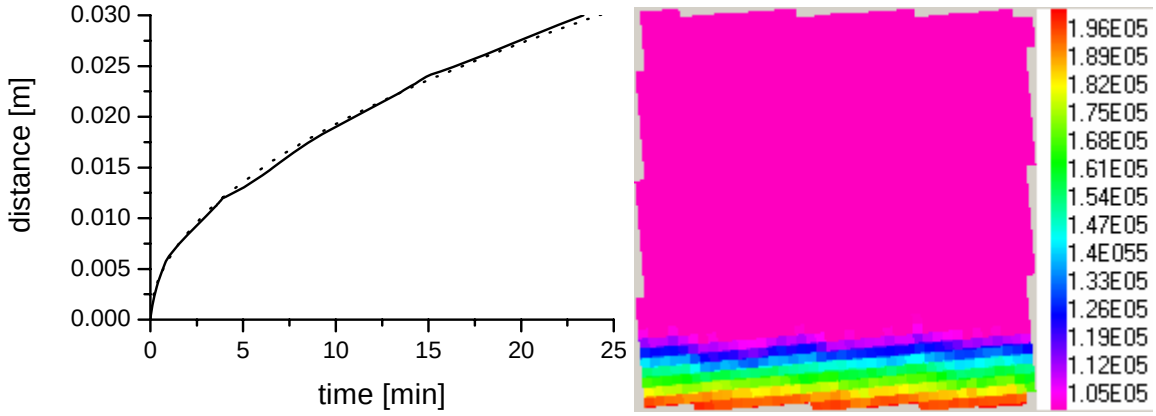

Fig. 3 Left: travelled distance (solid) of the fluid front and square root law (dotted) vs. time. Right: pressure (in [Pa]) on both sides of the impregnation front at the beginning.

EXAMPLES OF MOTION OF FLUID FRONT AND CREATION OF BUBBLES FOR SMALL WETTING FORCE

A system of oriented bundles with slight perturbation in each layer is now constructed in order to model a bi-axial fabric. For the simulations constant pressure values are assumed at the inlet and at the outlet of the system. The side walls are assumed as being isolated and no fluid can thus go through. The distance travelled by the fluid front is approximately proportional to the square root of time as shown in Fig. 3 left, because the pressure gradient decreases with time at fixed pressures of the inlet and outlet [12]. Small deviations from this law can occur because of perturbations and additional capillary pressure at the fluid front. The pressure distribution is shown in Fig. 3 right at the beginning of the impregnation. Of course, practically all of the pressure is lost over the fluid part of the system. A typical development of the fluid front that travel by the pressure gradient and the jumping of inter-bundle bubbles behind the fluid front are shown in Fig. 4. Simulations showed that common places of inter-bundle bubble trapping are at the edges, in small gaps and at crossings and threads. The fluid front moves faster in larger gaps implying that the capillary pressure is of less importance in these simulations.

Simulations showed that the number of intra-bundle bubbles usually exceeds the number of inter-bundle bubbles. However, the intra-bundle bubbles are much smaller in size and molar amount of gas is much less than inside the inter-bundle bubbles. The typical development of bubble count and their molar amount is shown in Fig. 5. The amount of bubbles is nearly the largest when fluid front reaches the output and least pressure gradient is achieved. Some of the trapped inter-bundle

bubbles starts to move only period after the fluid front have crossed the output. The molar amount of gas in bubbles varies more slowly because the largest contribution comes from large trapped bubbles and the fact that molecular transport of gas is currently absent in the model.

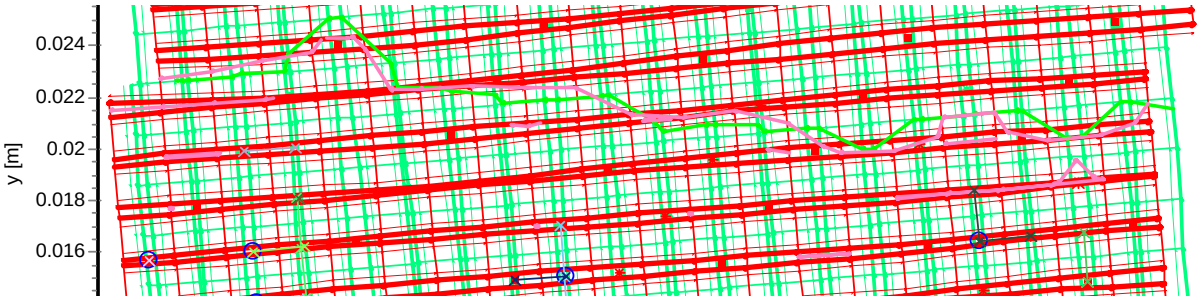

Fig. 4 Development of flow front as it moves upwards in the figure and jumping of formed bubbles behind the fluid front as blue circles. The upper two layers in the stack are shown.

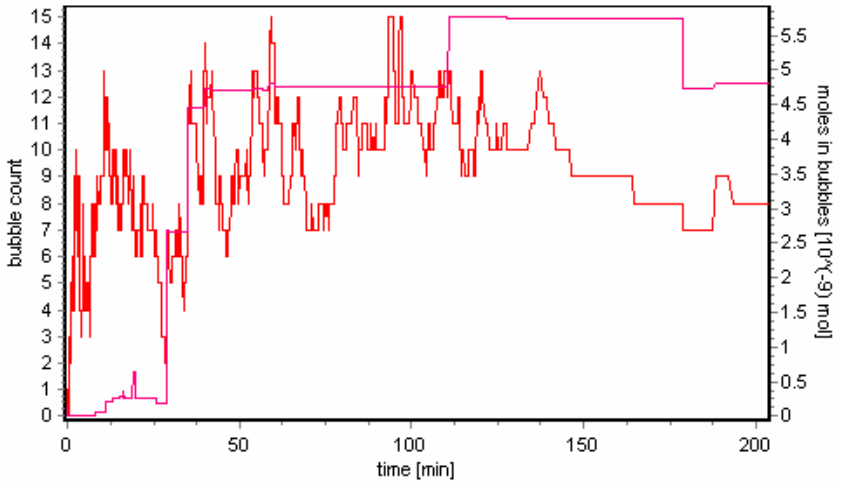

Fig. 5 Change of inter-bundle bubble count (quickly changing) and their amount in moles (slowly changing) during impregnation in small 4 cm × 5 cm system.

The profiles of void volume have been studied also experimentally [3] for a kind of unidirectional non crimp fabrics where most of the fibres are laid in straight bundles while a fraction of them is used to weave these bundles together (see Fig. 6). The major outcome of the experimental studies was that void fraction can be significantly reduced by reducing the pressure of outlet.

The same situation is now studied numerically for a bi-axial non-crimp by also reducing the pressure gradient to 0.25 MPa. Therefore, the void fraction of inter-bundle voids is reduced and the size of the plateau of significant void fraction is reduced. It must also be noticed that only the interbundle voids are considered and that the detailed geometry of the two fabrics studies differs. Still the model seems to capture the main mechanisms. Also, the small tail near the inlet occurs because the molecular transport of gas is currently absent in the model and trapped bubbles could stay for long. The characteristic positions of the voids are shown in Fig. 8. The flow is from the bottom to the top.

CONCLUSIONS

A 3D numerical model has been built for study of fluid front, creation of bubbles and bubble dynamics during impregnation of non-crimp fabrics. Elementary permeabilities through cell interfaces are included from independent approximations. It could be useful in study of quality of impregnating fabrics after impregnation. Currently only the inter-bundle voids are strictly considered. Numerical calculations showed that common places of intra-bundle bubble creation are tiny gaps between the bundles, crossings, threads, and side walls of the system. Numerical calculations confirmed experimental investigations that the remaining void fraction can be reduced by vacuum assistance at the outlet which is in agreement with experimental results.

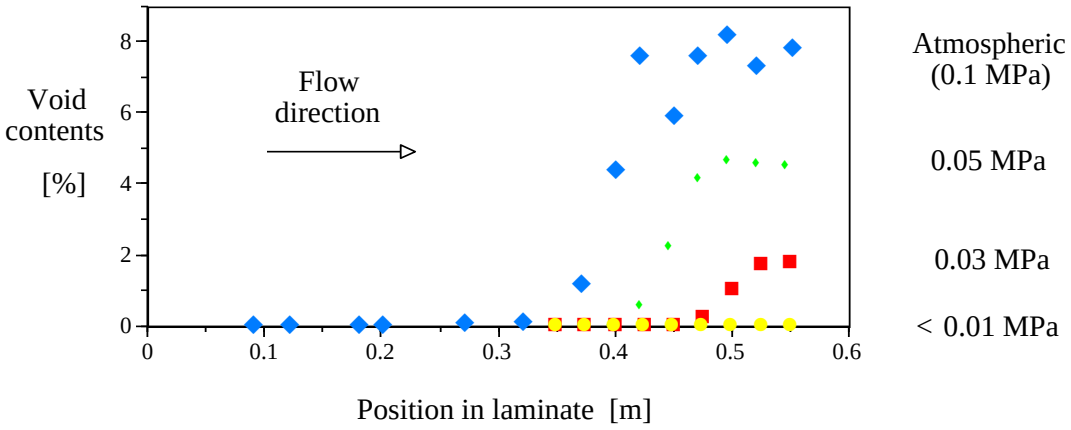

Fig. 6 Experimental void volume profiles [3] along the laminate centreline for a unidirectional fabric (Brochier Lyvertex 21130). Distance *x* is measured from the inlet towards the outlet. The pressure difference between inlet and outlet was 0.5 MPa and the outlet pressure was held at 0.1 MPa, 0.05 MPa, 0.01 MPa, and ≈ 0.001 MPa.

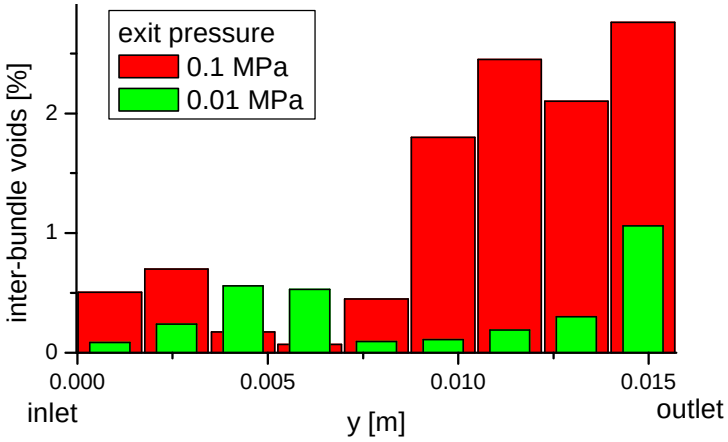

Fig. 7 Percentage of inter-bundle voids when fluid front has just passed the outlet. The pressure gradient was twice higher than in experiments in Fig. 6.

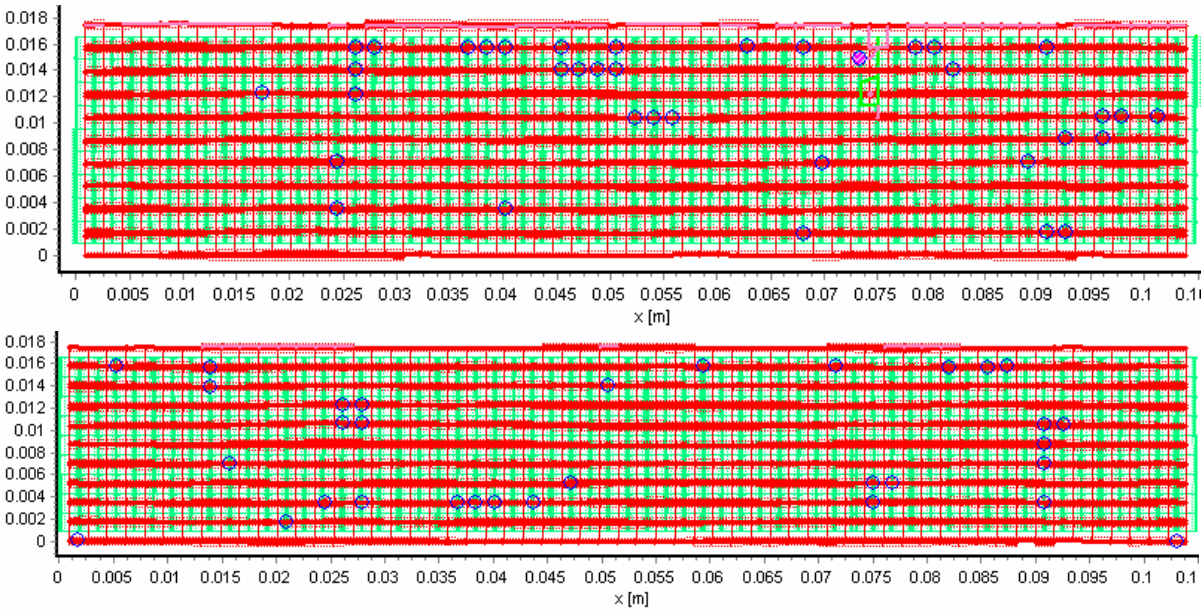

Fig. 8 Placement of inter-bundle bubbles in perturbed fabric when fluid front has just passed the outlet. Only the two uppermost layers of four are shown. Top: exit pressure is 0.1 MPa, bottom: exit pressure 0.01 MPa.

REFERENCES

1. R.S. Parnas, A.J. Salem, T.A. Sadiq, H.P. Wang and S.G. Advani, "Interaction between Micro- and Macroscopic Flows in RTM Preforms", *Composite Structures*, Vol. 27, 1994, pp. 93-107.

2. T.S. Lundström, H. Gustavsson, N. Jekabsons, A. Jakovics, "Dynamics of Wicking during Filling of Multi-Scale Porous Media: Porous Pore-Doublet Model, Experiments and Theory", *AIChE Journal*, Vol. 54, 2008, pp. 372-380.

3. T.S. Lundström and B.R. Gebart, "Influence from Process Parameters on Void Formation in Resin Transfer Molding", *Polymer Composites*, Vol. 15, 1994, pp. 25-33.

4. T.S. Lundström, B.R. Gebart and C.Y. Lundemo, "Void Formation in RTM", *Journal of Reinforced Plastics and Composites*, Vol. 12, 1993, pp. 1340–1349.

5. N. Patel, L.J. Lee, "Effects of Fiber Mat Architecture on Void Formation and Removal in Liquid Composite Molding", *Polymer Composites*, Vol. 16, 1995, pp. 386–399.

6. D.H. Lee, W.I. Lee and M.K. Kang, "Analysis and Minimization of Void Formation during Resin Transfer Molding Process", *Composites Science and Technology*, Vol. 66, 2006, pp. 3281-3289.

7. Y.K. Hamidi, L. Aktas and M.C. Altan, “Effect of Packing on Void Morphology in Resin Transfer Molded E-glass/Epoxy Composites”, *Polymer Composites*, Vol. 26, 2005, pp. 614-627.

8. T.S. Lundström, V. Frishfelds and A. Jakovics. “A Statistical Approach to Permeability of Clustered Fibre Reinforcements”, *Journal of Composite Materials*, Vol. 38, No. 13, 2004, pp. 1137-1149.

9. V. Frishfelds, T.S. Lundström and A. Jakovics, “Automatic Recognition and Analysis of Scanned Non-Crimp Fabrics for Calculation of their Fluid Flow Permeability”, *Journal of Reinforced Plastics and Composites*, Vol. 26, No. 3, 2007, pp. 285-296.

10. M. Nordlund, T.S. Lundström, V. Frishfelds and A. Jakovics. ”Permeability Network Model to Non-Crimp Fabrics”, *Composites Part A*, Vol. 37A, 2006, pp. 826-835.

11. T.S. Lundström and B.R. Gebart, “Effect of Perturbation of Fibre Architecture on Permeability Inside Fibre Tows”, *Journal of Composite Materials*, Vol. 29, 1995, pp. 424-443.

12. S.G. Advani and Z. Dimitrova, “Role of Capillary Driven Flow in Composite Manufacturing” in “*Surface and Interfacial tension: Measurement, Theory and Applications*”, Edt. S. Hartland, Marcel Dekker inc., New York, 2004, pp. 263-311.

13. V. Frishfelds, T.S. Lundström and A. Jakovics, “Lattice-Gas Analysis of Fluid Front in Non-Crimp Fabrics”, *The 19th International Symposium on Transport Phenomena, 17-20 August, 2008, Reykjavik, Iceland*.

14. V. Frishfelds, T.S. Lundström and A. Jakovics, ”Bubble Motion through Non-Crimp Fabrics during Composites Manufacturing”, *Composites Part A*, Vol. 39, No. 2, 2008, pp. 243-251.